






Original Research

A Real-Time Driver Drowsiness Detection Method Using a Hybrid of Deep Learning and Fuzzy Logic

Amir Sohrabinezhad¹ , Reza Sabbaghi-Nadooshan^{1,*} , Nasser Talebi² ,
Roohollah Barzamini¹ , Fardad Farokhi³ 

¹Department of Electrical Engineering, CT.C, Islamic Azad University, Tehran, Iran

²Department of Electrical Engineering, YI.C, Islamic Azad University, Tehran, Iran

³Department of Biomedical Engineering, CT.C, Islamic Azad University, Tehran, Iran

*Corresponding author: r.sabbaghi@iau.ac.ir

Article History

Received:

31 August 2025

Revised:

28 November 2025

Accepted:

1 January 2026

Published in Issue:

30 June 2026

© 2026 The Author(s). Published by the OICC Press under the terms of the [CC BY 4.0, Creative Commons Attribution License](https://creativecommons.org/licenses/by/4.0/), which permits use, distribution and reproduction in any medium, provided the original work is properly cited.

Abstract:

Driver drowsiness contributes to approximately 21% of traffic accidents. Three deep neural networks were trained, with ResNet50 achieving the best performance: 99.74% training accuracy, 99.62% validation accuracy, an average test F1-score of 0.99, no overfitting, and real-time inference at 0.023 seconds per frame on an RTX 3060 laptop GPU with 6GB RAM. Following drowsiness detection, a fuzzy inference system integrating Eye Aspect Ratio (EAR) and Mouth Aspect Ratio (MAR) is applied to determine the drowsiness severity. The system was tested with an infrared camera on 453 volunteers from various Middle Eastern ethnic groups under different lighting conditions. A local database was compiled from these tests, recording 31 misclassifications and achieving an overall accuracy of 93.16%. The findings demonstrate that the system performs reliably under both day and night conditions and across diverse ethnicities, supporting its suitability for integration into advanced driver-assistance systems (ADAS).

Keywords: Real-time drowsiness detection; Determining the degree of drowsiness; Deep learning; Fuzzy inference systems

Cite this article: Sohrabinezhad A, Sabbaghi-Nadooshan R, Talebi N, Barzamini R, Farokhi F. A Real-Time Driver Drowsiness Detection Method Using a Hybrid of Deep Learning and Fuzzy Logic. *Majlesi J. Electr. Eng.* 2026;20(2): 209-228. <https://doi.org/10.57647/mjee.2026.2002.15>

1. Introduction

Drowsiness is a leading factor in road accidents, causing significant human and economic losses. To address this issue, advanced approaches such as deep neural networks, machine learning algorithms, and intelligent paradigms like fuzzy logic have been applied, all with the objective of improving real-time detection accuracy and activating in-vehicle audio alerts to keep drivers awake. The present study integrates intelligent techniques with large-scale field testing to deliver comprehensive results. Beyond detection accuracy, the system also evaluates frame-level real-time processing performance, enabling a joint assessment of both speed and precision. One common implementation strategy for drowsiness detection systems utilizes convolutional neural networks (CNNs), such as

VGG16 [1], one of the effective approaches in training deep neural networks is the use of transformer-based architectures, which offer highly favorable accuracy and performance [2, 3], as well as other architectures [4, 5, 6, 7, 8, 9, 10, 11, 12, 13, 14, 15], which have shown high accuracy rates. A traditional PERCLOS-based method was also employed for drowsiness detection [16]. Eye closure and yawning detection are implemented using the dlib library and Python [17, 18]. Both dlib and OpenCV are widely employed in Python-based driver monitoring systems [19]. Research indicates that around 21% of all road accidents are associated with driver fatigue. To improve image quality and detection performance, Support Vector Machine (SVM) classifiers and Histogram of Oriented Gradients (HOG) features are often combined with dlib and OpenCV frameworks

[20]. Validation is performed through live video streams and dedicated databases [21]. Further improvements to the traditional convex hull algorithm have been proposed via advanced filtering methods [22]. Additionally, facial feature localization is achieved through machine learning-based recognition of 68 key landmarks [23, 24]. Fuzzy logic is then applied to interpret eye activity, providing an estimation of drowsiness levels [25, 26, 27, 28]. Fuzzy logic is employed in various systems characterized by uncertainty in categorized values [29, 30, 31, 32, 33]. One specialized domain where fuzzy logic proves particularly effective is image processing [34, 35, 36, 37].

2. Proposed method

At the initial stage, three neural networks were trained on a drowsiness dataset containing two labels: Normal and Drowsiness. A performance comparison was carried out among these networks and findings from related studies. The most suitable network was selected based on training accuracy, validation outcomes, test performance, and real-time inference capability on an RTX 3060 laptop GPU with 6GB RAM. The chosen model was then integrated with an image processing approach utilizing Eye Aspect Ratio (EAR) and Mouth Aspect Ratio (MAR) features, combined with a fuzzy logic system to estimate the degree of driver drowsiness. The developed system was validated in field experiments with 453 participants of diverse ethnic origins from the Middle East. Live camera testing confirmed the reliability of the proposed framework. The complete block diagram of the system is presented in Fig. 1, while the recommended in-vehicle camera installation point is depicted in Fig. 2 (a). An image captured from this installation position is shown in Fig. 2 (b).

The research gaps identified through the review of similar studies highlight the necessity of conducting this research (Table 1). The combination of the model

trained with the ResNet50 deep neural network, together with EAR/MAR-based fuzzy inference and its validation on 453 volunteers in live tests, demonstrated that the proposed hybrid method effectively addresses the gaps left by previous approaches.

2.1 Convolutional neural networks for drowsiness detection

For the implementation of all neural networks in this study, a publicly available and free drowsiness dataset was utilized, accessible at:

(<https://universe.roboflow.com/ltomic01/driver-drowsiness-detection-gk0ws/dataset/1/download>).

This dataset, divided into two categories with class labels Normal and Drowsiness, was used for training, validation, and testing. The original image dimensions were 640×640 pixels, and all images were resized to 224×224 pixels before being fed into the networks. Model training was conducted on an RTX 3060 laptop GPU with 6GB of RAM. The initial configuration parameters for each network are summarized in Table 2. The default number of training epochs for all neural networks used in this study was set to 50. However, a common condition was applied for all three networks: if the training results became stable and repetitive, training would be stopped. Consequently, the ResNet50 neural network was trained for only 23 epochs, while the ViT-Tiny network completed 13 training epochs. The specifications of the dataset used, along with the applied configurations, are presented in Table 3.

The collected dataset obtained from the field tests was captured using a camera whose technical specifications are presented in Table 4. The distance between the camera and the subject during field testing and database collection was set between 30 and 80 centimeters to ensure that the camera and the system could be installed in vehicles of various sizes.

A computer vision system is considered real-time if

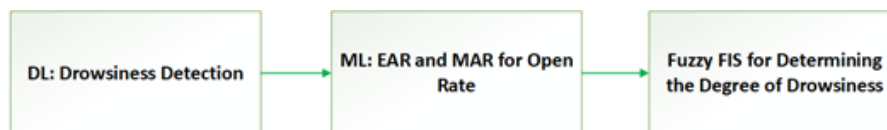


Figure 1. Overall block diagram of the proposed architecture.



Figure 2. (a) Recommended camera mounting location, (b) Image acquired from the recommended mounting position.

Table 1. Distinctive of the research.

| Distinctive of the research | Description |
|--|---|
| Use of the same hardware for training and testing | All neural network training and tests were conducted on the model obtained from extracting the best neural network using the same hardware. |
| Combining neural network with fuzzy logic | Drowsiness detection accuracy was improved by integrating the model extracted from neural network training with fuzzy logic. |
| Conducting tests in a real environment with diverse volunteers | The study was performed to obtain real results, including volunteers from different ethnic backgrounds. |
| Applicability in the automotive industry | The research results can confidently be applied in Advanced Driver Assistance Systems (ADAS). |
| Addressing identified research gaps | The table explicitly highlights research gaps (e.g., lack of large-scale field validation, limited ethnic diversity in datasets, absence of fuzzy logic integration) and clarifies how our work addresses them. |

Table 2. Fractions of non-cellulose polysaccharides of CS.

| Parameters | Values |
|----------------------------------|----------------------------|
| Hardware-GPU | RTX3060-laptop, 6GB of RAM |
| Real-Time Threshold | 0.04 s |
| Image dimensions in the dataset | 640 × 640 |
| Image dimensions during training | 224 × 224 |
| Learning-rate | 1e-4 |
| Batch-size | 32 |
| Num-epochs | 50 |

Table 3. Complete dataset specifications.

| Feature | Description |
|--------------------|--|
| Dataset name | Driver Drowsiness Detection (Roboflow, Itomic01) |
| Total size | 1448 images |
| Number of classes | 2 (Normal, Drowsiness) |
| Class distribution | Number of images labeled as drowsy used for training: 500. Number of images labeled as normal used for training: 513. Number of images labeled as drowsy used for testing: 74. Number of images labeled as normal used for testing: 72. Number of images labeled as drowsy used for validation: 145. Number of images labeled as normal used for validation: 144. |
| Data splits | Training: 70% (1013 images), Validation: 20% (289 images), Test: 10% (146 images) |
| Preprocessing | All images were resized to 224 × 224 pixels and converted to tensor format |
| Data augmentation | No augmentation was applied |

Table 4. The parameters configured for the camera capturing the driver's images.

| Specification | Values |
|-------------------------|--|
| Appearance type | Bullet |
| Connection type | Wired (LAN), Wireless (Wi-Fi) |
| Image sensor type | CMOS |
| Shutter speed range | 1/3 s – 1/100,000 s |
| Supported resolutions | 1080p (1920×1080), 1.3MP (1280×960), 720p (1280×720), VGA (640×480), QVGA (320×240) |
| Night Vision Capability | Yes |
| Optical Zoom | ×1 |
| Digital Zoom | ×16 |
| Viewing Angle | Horizontal: 106°, Vertical: 56°, Diagonal: 135.6° – and also Horizontal: 93°, Vertical: 48°, Diagonal: 114.8° |
| Minimum Illumination | 0.0275 Lux @F2.0 (Color, 80 IRE); 0.0134 Lux @F2.0 (B/W, 80 IRE); 0 Lux (IR on). Also: 0.1983 Lux @F2.0 (Color, 80 IRE); 0.1128 Lux @F2.0 (B/W, 80 IRE); 0 Lux (IR on) |
| IR Night Vision Details | Smart IR up to 30 meters |
| Supported Storage | Micro SD up to 256 GB |

it processes each video frame within a time less than or equal to the interval between two consecutive frames, satisfying the real-time constraint (equation (1)).

$$\begin{cases} T_{\text{inference}} \leq \Delta t, \\ \Delta t = \frac{1}{f_{fps}}, \end{cases} \Rightarrow T_{\text{inference}} \leq \frac{1}{f_{fps}} \quad (1)$$

where

$T_{\text{inference}}$: Time to process one frame (inference time)

Δt : Time between two frames

f_{fps} : Frame rate of the video (frames per second)

Given that 25 frames per second are received from the camera for processing, each frame therefore requires 0.04 seconds to be processed. This duration represents the maximum time that can be considered as the real-time threshold.

$$T_{\text{inference}} \leq \Delta t \Rightarrow T_{\text{inference}} \leq \frac{1}{25} = 0.04 \text{ s}$$

The F1-score was calculated based on the validation set using the standard definition to assess the neural network's classification performance (equation (2)) [3, 11].

$$\text{F1-Score} = 2 \times \frac{\text{Precision} \times \text{Recall}}{\text{Precision} + \text{Recall}} \quad (2)$$

The resulting F1-Score is always a number between 0 and 1. A value close to 0 indicates that the model performed poorly, while a value close to 1 indicates that the model was accurate and missed very few cases.

In the first supervised training, performed using the ResNet-50 network, the model was trained with the

Adam optimizer and the cross-entropy loss function. The network was trained for 23 epochs, achieving an average training accuracy of 99.74% and an average validation accuracy of 99.62% (Fig. 3). In the real-time inference processing test, an average processing time of 0.023 seconds per frame was obtained, indicating that the processing was performed within the real-time range on the GPU (Fig. 4).

In the second supervised training, conducted using the MobileNetV3 network, the network was trained for 50 epochs, achieving an average training accuracy of 99.08% and an average validation accuracy of 96.84% (Fig. 5). In the real-time inference processing test, an average processing time of 0.021 seconds per frame was obtained, indicating that the processing was not performed within the real-time range on the GPU (Fig. 6).

In the third supervised training, conducted using the vit-tiny network, the network was trained for 13 epochs, achieving an average training accuracy of 98.62% and an average validation accuracy of 98.46% (Fig. 7). In the real-time inference processing test, an average processing time of 0.020 seconds for most frames and up to 0.022 seconds for some frames was obtained, indicating that the processing was not performed within the real-time range on the GPU (Fig. 8).

The three neural networks examined in this study demonstrate differences in performance. The evaluation results, along with the corresponding output charts, are presented to illustrate the models' accuracy (Figs. 9, 10, and 11).

The comparative analysis of ResNet50 performance on the training and validation datasets, as shown in Fig. 9,

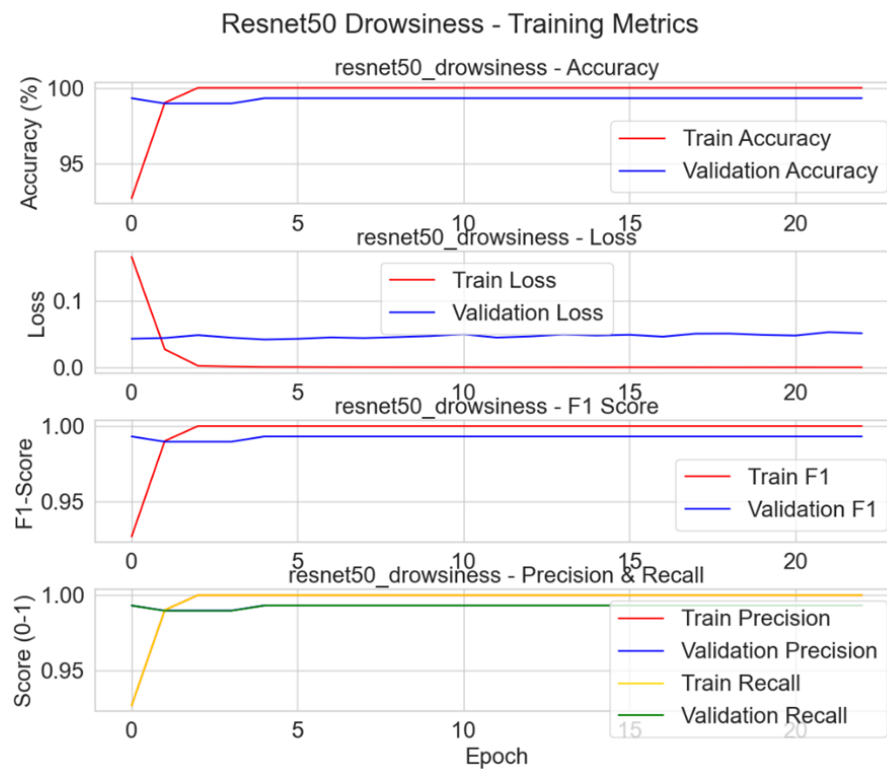


Figure 3. Training accuracy and loss chart (ResNet50).

highlights the model's strong generalization capability. The training accuracy is 99.74%, while the validation accuracy is 99.62%, indicating that the model effectively learns discriminative features without significant overfitting. Similarly, the precision, recall, and F1-score for both datasets are nearly identical and all reach approximately 99%. This balanced performance across the evaluation metrics demonstrates that the model is equally effective in minimizing false positives and false negatives, thereby providing reliable detection of both drowsy and normal states. The negligible gap between training and validation performance further confirms the

model's robustness when exposed to unseen data. Such stability is particularly important for safety-critical applications such as driver monitoring, where both sensitivity to drowsiness and avoidance of false alarms are essential. Overall, these results validate ResNet50 as a dependable and well-generalized architecture for real-time driver drowsiness detection (Fig. 9).

The comparative performance analysis of MobileNetV3-Small on the training and validation datasets, as illustrated in Fig. 10, highlights the model's strong generalization capability. The training accuracy is 99.08%, while the validation accuracy is 96.84%,

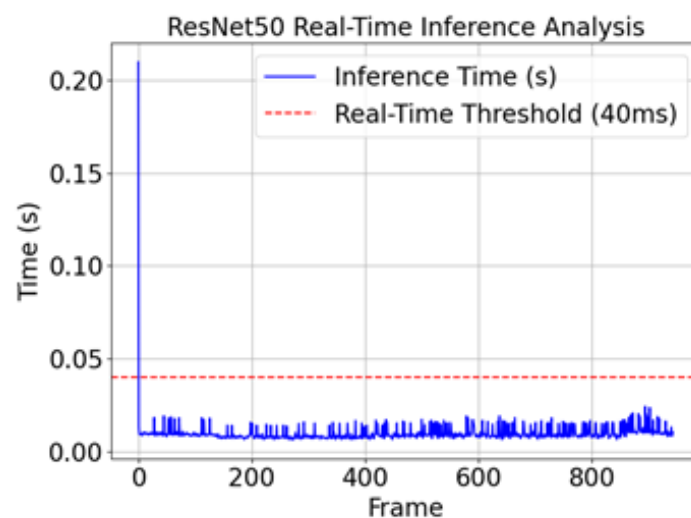


Figure 4. Real-time test output (ResNet50 Inference).

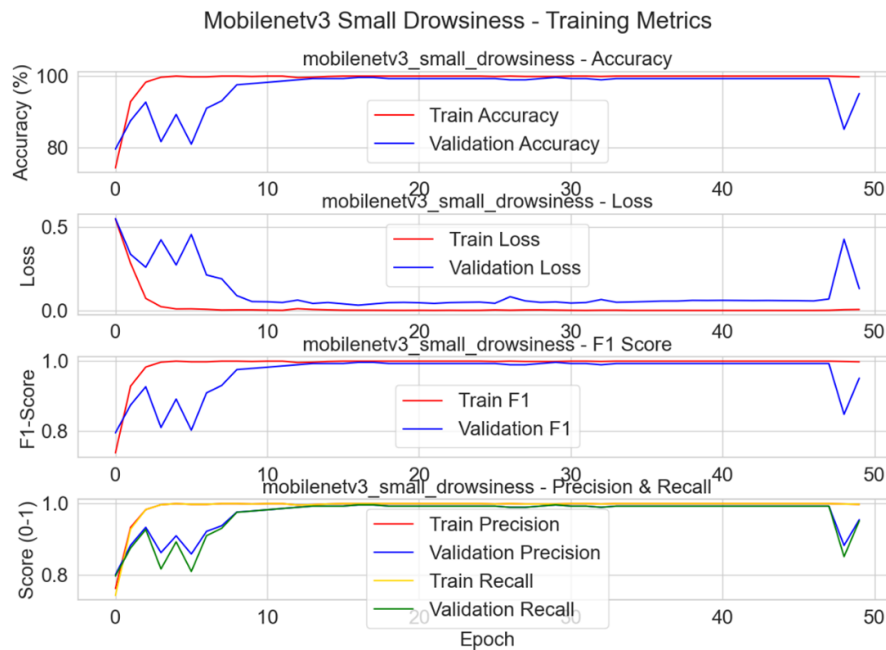


Figure 5. Training accuracy and loss chart (MobilenetV3).

which shows a noticeable decrease compared to the validation accuracy achieved by the ResNet50 neural network. Similarly, the precision, recall, and F1-score metrics exhibit identical and closely matched values for both datasets. The recall value is 96%, and the precision value is 97%, and the F1-score is 96.49%. This nearly balanced performance across all metrics indicates that the model is equally effective in reducing false positives and false negatives; however, it does not ensure as reliable discrimination between drowsy and normal states as the ResNet50 network (Fig. 10).

The comparative performance analysis of ViT-Tiny on the training and validation datasets, as illustrated in Fig. 11, highlights the model's strong generalization capability. The training accuracy is 98.62%, while the

validation accuracy is 98.46%, indicating a slight decrease compared to the validation accuracy achieved by the ResNet50 neural network. Similarly, the precision, recall, and F1-score metrics exhibit nearly identical values across both datasets. The recall is 98%, the precision is 98%, and the F1-score is 98%. This nearly balanced performance across all metrics demonstrates that the model is equally effective in reducing false positives and false negatives; however, it does not guarantee as reliable discrimination between drowsy and normal states as the ResNet50 network (Fig. 11).

At the conclusion of the evaluation of the selected neural networks in this study, confusion matrix figures (Figs. 12, 13, and 14) were added for the trained hybrid model systems, illustrating the distribution of true posi-

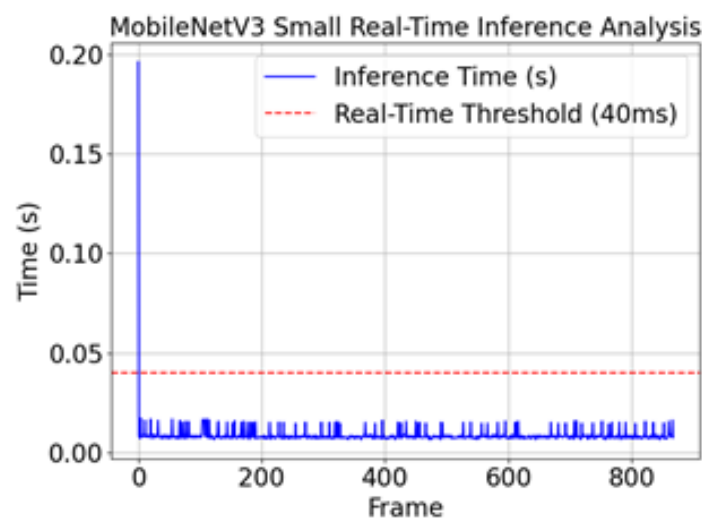


Figure 6. Real-time test output (MobilenetV3).

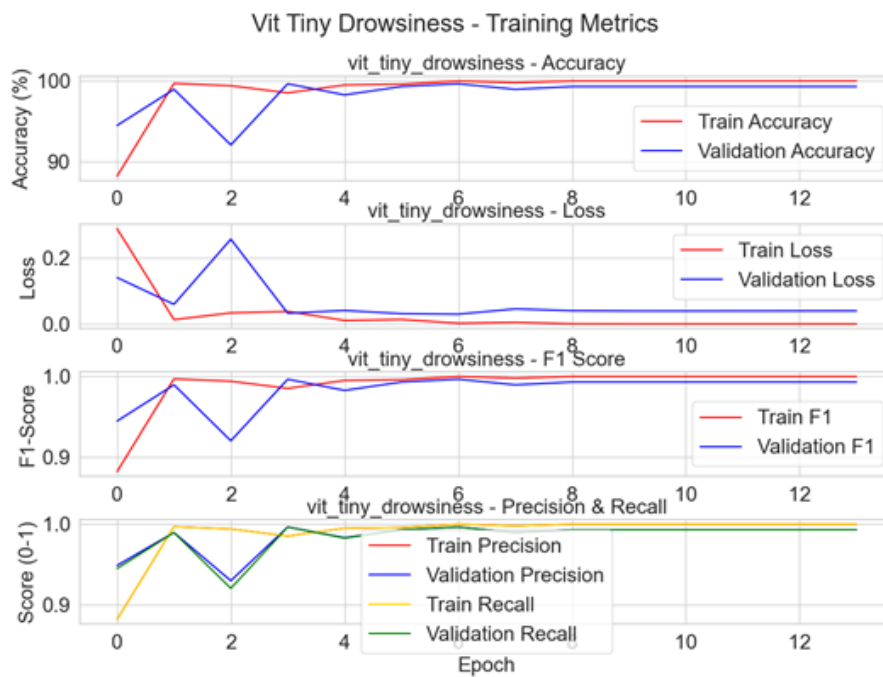


Figure 7. Training accuracy and loss chart (ViT-Tiny).

tives, false positives, true negatives, and false negatives. These figures provide clearer insight into the types of errors observed during the validation of each model.

The confusion matrix of the ResNet50 model clearly illustrates its classification performance. Out of a total of 289 test samples, the model correctly identified 144 drowsy cases and 143 normal cases. One drowsy sample was incorrectly classified as normal (false negative), and one normal sample was incorrectly classified as drowsy (false positive). Overall, the network demonstrates very high accuracy (Fig. 12).

The confusion matrix of the MobileNetV3-Small model clearly illustrates its classification performance. Out of a total of 289 test samples, the model correctly identified 139 drowsy cases and 140 normal cases, while

6 drowsy samples were incorrectly classified as normal (false negatives) and 4 normal samples were incorrectly classified as drowsy (false positives). These statistics indicate that, compared to the ResNet50 model, this network exhibits a higher number of classification errors (Fig. 13).

The confusion matrix of the ViT-Tiny model clearly illustrates its classification performance. Out of a total of 289 test samples, the model correctly identified 142 drowsy cases and 141 normal cases, while 3 drowsy samples were incorrectly classified as normal (false negatives) and 3 normal samples were incorrectly classified as drowsy (false positives). These statistics indicate that, compared to the ResNet50 model, this network exhibits a slightly higher number of classification errors (Fig. 14).

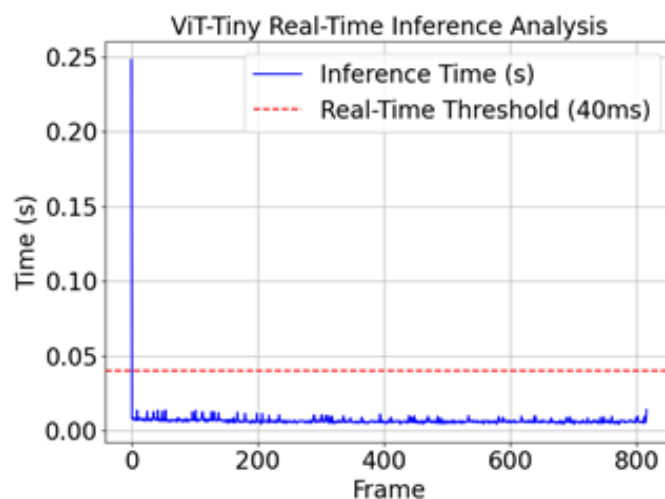


Figure 8. Real-time test output (ViT-Tiny).

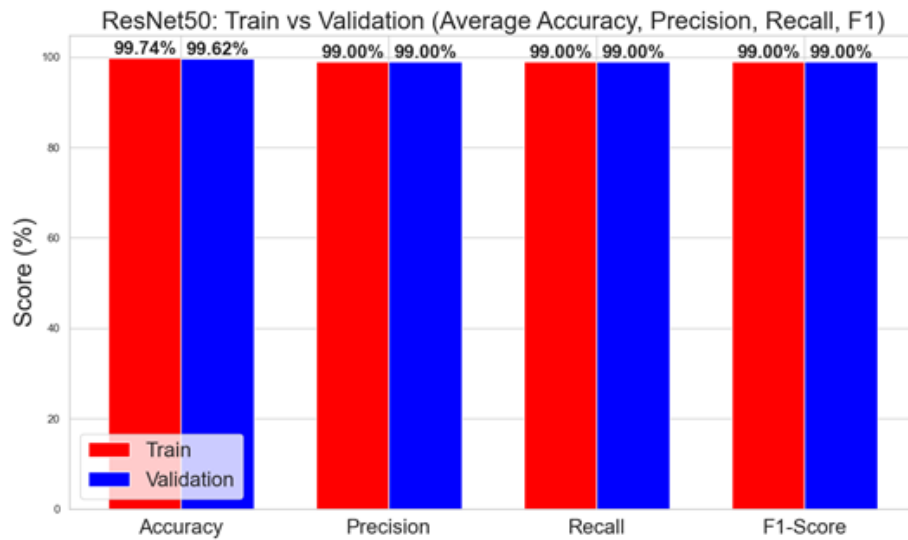


Figure 9. Comparison of train and validation in the ResNet50 neural network.

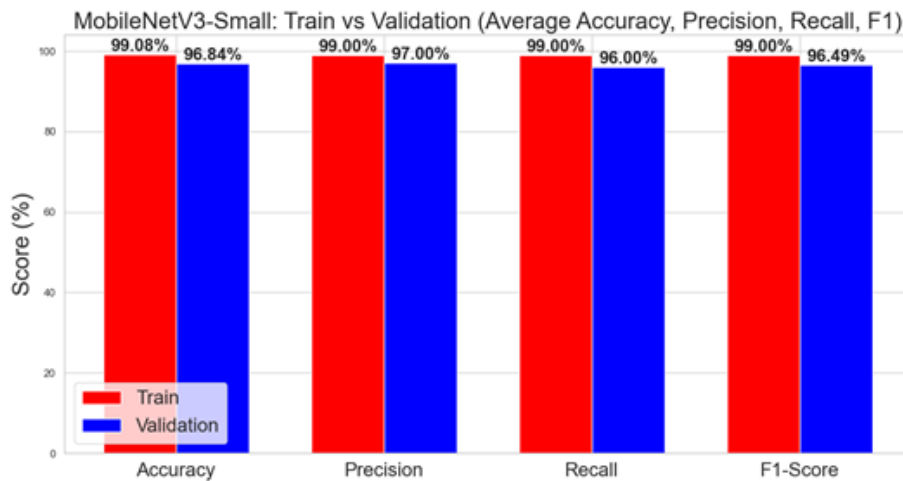


Figure 10. Comparison of train and validation in the MobileNetV3 neural network.

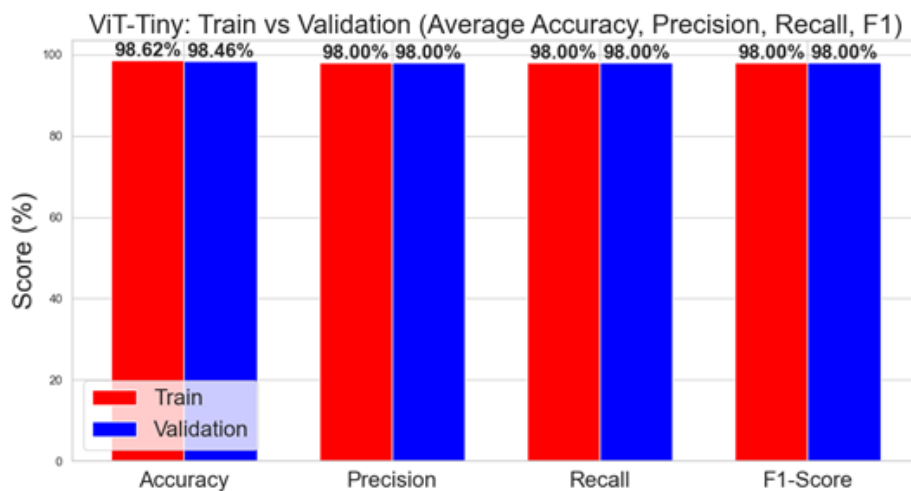


Figure 11. Comparison of train and validation in the ViT-Tiny neural network.

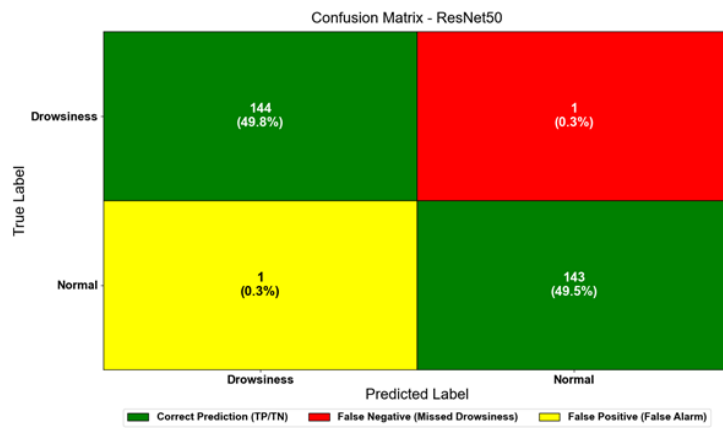


Figure 12. Confusion matrix for ResNet50.

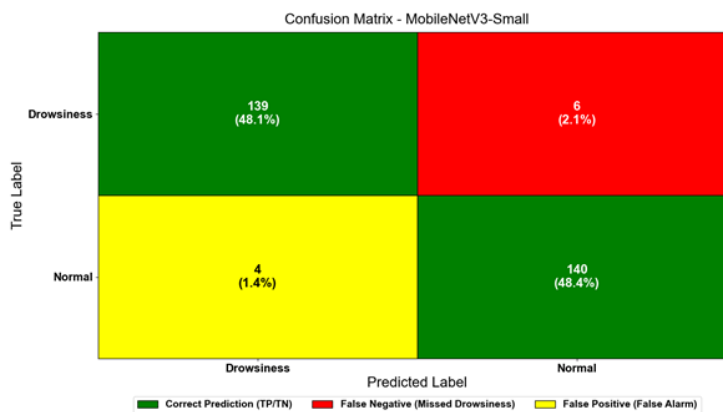


Figure 13. Confusion matrix for MobileNetV3.

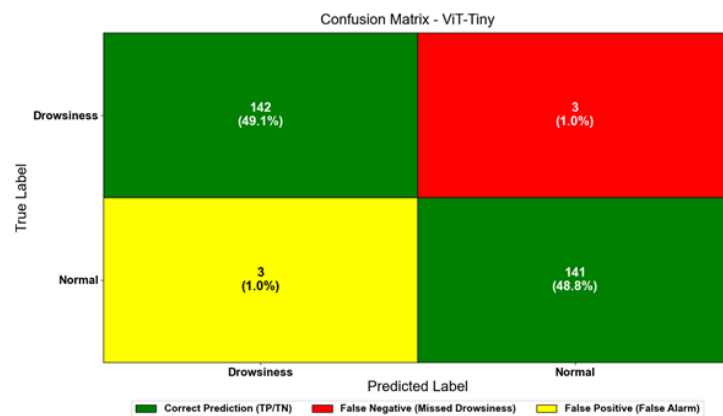


Figure 14. Confusion matrix for ViT-Tiny.

2.2 Drowsiness level assessment

The “shape_predictor_68_face_landmarks.dat” dataset was employed to extract 68 facial landmarks (Fig. 15 and Table 5). Using these landmarks, the Eye Aspect Ratio (EAR) and Mouth Aspect Ratio (MAR) metrics were calculated to measure eye closure and mouth opening, respectively, for estimating the severity of drowsiness (equation (3)). This approach introduces two primary challenges. The first challenge is normal blinking, where certain individuals naturally exhibit a higher frequency or longer duration of eyelid closure, which may be

misinterpreted as drowsiness. The second challenge arises when the driver engages in conversation with passengers, as mouth movements during speech can resemble yawning, potentially leading to false detections. To mitigate these issues, the Mamdani fuzzy inference method was integrated with EAR and MAR analysis in this study. A further challenge is the variability of facial features among individuals from different ethnic groups. To overcome this, extensive field tests were conducted across diverse ethnic populations, generating a localized database from real-world experiments. The outcomes of

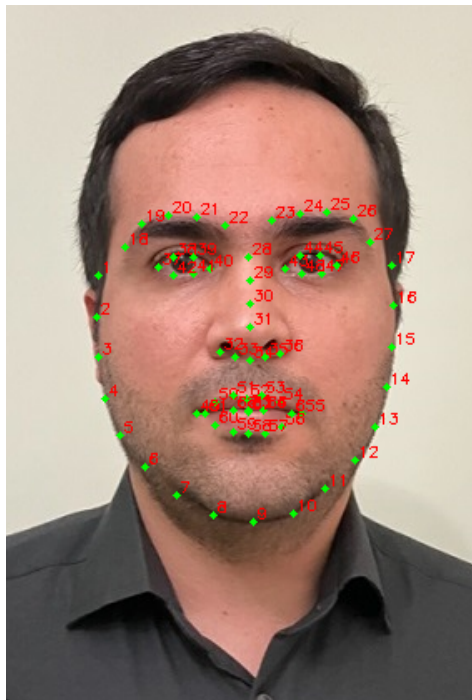


Figure 15. Detecting 68 facial landmarks.

these comprehensive tests validated the robustness and high accuracy of the proposed system.

$$\begin{cases}
 \text{EAR}_{\text{Right_eye}} = \frac{\|P_{38}-P_{42}\|+\|P_{39}-P_{41}\|}{2\|P_{37}-P_{40}\|} \\
 \text{EAR}_{\text{Left_eye}} = \frac{\|P_{44}-P_{48}\|+\|P_{45}-P_{47}\|}{2\|P_{43}-P_{46}\|} \\
 \Rightarrow \text{EAR} = \left(\frac{\text{EAR}_{\text{Right_eye}} + \text{EAR}_{\text{Left_eye}}}{2} \right) \\
 \left\{ \begin{array}{l} M_1 = P_{49} \\ M_8 = P_{55} \end{array} \right. \\
 \text{Average}_{\text{Upper_lip}} = \begin{cases} M_3 = \frac{|P_{51}-P_{62}|}{2} \\ M_5 = \frac{|P_{52}-P_{63}|}{2} \\ M_7 = \frac{|P_{53}-P_{64}|}{2} \end{cases} \\
 \text{Average}_{\text{Lower_lip}} = \begin{cases} M_2 = \frac{|P_{57}-P_{66}|}{2} \\ M_4 = \frac{|P_{58}-P_{67}|}{2} \\ M_6 = \frac{|P_{59}-P_{68}|}{2} \end{cases} \\
 \Rightarrow \text{MAR} = \frac{\|M_3 - M_2\| + \|M_5 - M_4\| + \|M_7 - M_6\|}{3\|M_1 - M_8\|}
 \end{cases} \quad (3)$$

The membership functions of the fuzzy variables EAR and MAR were defined to describe their degrees of membership (equation (4)), while the resulting fuzzy membership functions from the combined EAR and MAR rules were derived based on these definitions (equation (5)). Taking into account the driver’s eye condition-classified into three states: open, closed, and semi-closed-and the mouth condition-classified as closed, open, and semi-open-three fuzzy membership functions were defined for the eyes and three for the mouth. By combining these membership functions and formulating fuzzy rules, nine unique states were established, providing a complete set of rules for assessing the driver’s drowsiness level. The parameters of these membership functions were determined based on regular partitioning and practical experience (equations (4) and (5)). Validation of the fuzzy inference results using sensitivity analysis indicates the high accuracy of the selected membership function parameters.

$$\begin{aligned}
 \mu_{\text{EAR}(\text{Closed eye})}(x) &: \begin{cases} 1 & 0 \leq x \leq 0.2 \\ 1-x & 0.2 < x < 0.5 \\ 0 & 0.5 \leq x \leq 1 \end{cases} \\
 \mu_{\text{EAR}(\text{Semi Closed})}(x) &: \begin{cases} 0 & 0 \leq x \leq 0.2 \\ x+1 & 0.2 < x < 0.5 \\ 1-x & 0.5 \leq x < 0.8 \\ 0 & 0.8 \leq x \leq 1 \end{cases} \\
 \mu_{\text{EAR}(\text{Open})}(x) &: \begin{cases} 0 & 0 \leq x \leq 0.5 \\ x+1 & 0.5 < x < 0.8 \\ 1 & 0.8 \leq x \leq 1 \end{cases} \\
 \mu_{\text{MAR}(\text{Normal})}(x) &: \begin{cases} 1 & 0 \leq x \leq 5 \\ 1-x & 5 < x < 15 \\ 0 & 15 \leq x \leq 30 \end{cases} \\
 \mu_{\text{MAR}(\text{Medium})}(x) &: \begin{cases} 0 & 0 \leq x \leq 5 \\ x+1 & 5 < x < 15 \\ 1-x & 15 < x < 25 \\ 0 & 25 \leq x \leq 30 \end{cases} \\
 \mu_{\text{MAR}(\text{yawn})}(x) &: \begin{cases} 0 & 0 \leq x \leq 15 \\ x+1 & 15 < x < 25 \\ 1 & 25 \leq x \leq 30 \end{cases} \quad (4)
 \end{aligned}$$

Table 5. Detecting eyes and mouth.

| Name of the detected points | Number of points |
|---------------------------------|------------------|
| Right eye | 37-42 |
| Left eye | 43-48 |
| The upper line of the upper lip | 51-53 |
| Bottom line of the lower lip | 57-59 |
| Bottom line of the upper lip | 62-64 |
| The upper line of the lower lip | 66-68 |

Mamdani fuzzy rules for determining the level of drowsiness by combining EAR and MAR:

Considering that three fuzzy membership functions were defined for EAR and three for MAR, representing the driver's eye closure and mouth status respectively, the combination of these two sets of membership functions resulted in a maximum of nine fuzzy rules.

1. Rule 1: If EAR is closed and MAR is normal, then the drowsiness level is asleep.
2. Rule 2: If EAR is closed and MAR is yawning, then the drowsiness level is very high (vh).
3. Rule 3: If EAR is closed and MAR is medium, then the drowsiness level is high (h).
4. Rule 4: If EAR is semi closed and MAR is yawning, then drowsiness level is medium high (mh).
5. Rule 5: If EAR is semi closed and MAR is medium, then the drowsiness level is medium (m).
6. Rule 6: If EAR is semi closed and MAR is normal, then the drowsiness level is medium low (ml).
7. Rule 7: If EAR is open and MAR is yawning, then the drowsiness level is low (l).
8. Rule 8: If EAR is open and MAR is medium, then the drowsiness level is very low (vl).
9. Rule 9: If EAR is open and MAR is normal, then the drowsiness level is awake (a).

$$\mu_a(x) : \begin{cases} 1 & 0 \leq x \leq 0.1 \\ 1 - x & 0.1 < x < 0.2 \\ 0 & 0.2 \leq x \leq 1 \end{cases}$$

$$\mu_{vl}(x) : \begin{cases} 0 & 0 \leq x \leq 0.1 \\ x + 1 & 0.1 < x < 0.2 \\ 1 - x & 0.2 \leq x < 0.3 \\ 0 & 0.3 \leq x \leq 1 \end{cases}$$

$$\mu_l(x) : \begin{cases} 0 & 0 \leq x \leq 0.2 \\ x + 1 & 0.2 < x < 0.3 \\ 1 - x & 0.3 \leq x < 0.4 \\ 0 & 0.4 \leq x \leq 1 \end{cases}$$

$$\mu_{ml}(x) : \begin{cases} 0 & 0 \leq x \leq 0.3 \\ x + 1 & 0.3 < x < 0.4 \\ 1 - x & 0.4 \leq x < 0.5 \\ 0 & 0.5 \leq x \leq 1 \end{cases}$$

$$\mu_m(x) : \begin{cases} 0 & 0 \leq x \leq 0.4 \\ x + 1 & 0.4 < x < 0.5 \\ 1 - x & 0.5 \leq x < 0.6 \\ 0 & 0.6 \leq x \leq 1 \end{cases}$$

$$\mu_{mh}(x) : \begin{cases} 0 & 0 \leq x \leq 0.5 \\ x + 1 & 0.5 < x < 0.6 \\ 1 - x & 0.6 \leq x < 0.7 \\ 0 & 0.7 \leq x \leq 1 \end{cases}$$

$$\mu_h(x) : \begin{cases} 0 & 0 \leq x \leq 0.6 \\ x + 1 & 0.6 < x < 0.7 \\ 1 - x & 0.7 \leq x < 0.8 \\ 0 & 0.8 \leq x \leq 1 \end{cases}$$

$$\mu_{vh}(x) : \begin{cases} 0 & 0 \leq x \leq 0.7 \\ x + 1 & 0.7 < x < 0.8 \\ 1 - x & 0.8 \leq x < 0.9 \\ 0 & 0.9 \leq x \leq 1 \end{cases}$$

$$\mu_{asleep}(x) : \begin{cases} 0 & 0 \leq x \leq 0.8 \\ x + 1 & 0.8 < x < 0.9 \\ 1 & 0.9 \leq x \leq 1 \end{cases} \quad (5)$$

The sensitivity function of the above fuzzy rules serves as a criterion for validating the rules (Fig. 16).

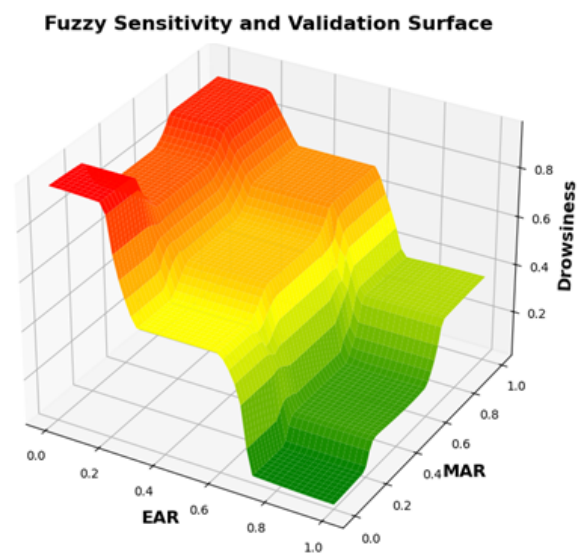


Figure 16. Fuzzy sensitivity and validation surface.

The three-dimensional surface illustrates the relationship between the input variables Eye Aspect Ratio (EAR) and Mouth Aspect Ratio (MAR) and the output variable representing the degree of drowsiness in the proposed fuzzy inference system. This surface enables a detailed examination of how the system models individual and joint effects of the two behavioral indicators on the final decision.

The output surface demonstrates that EAR is the most influential variable in determining the drowsiness level. When EAR lies within the range of 0 to approximately 0.2, the output remains consistently high and close to 1, regardless of the MAR value. This indicates that eye closure strongly activates the fuzzy rules associated with severe drowsiness.

As EAR increases beyond 0.35, the output decreases noticeably and stabilizes between 0.2 and 0.4, reflecting a

clear association between open eyes and a low probability of drowsiness. This behavior confirms that the system correctly prioritizes eye-related indicators as primary contributors to drowsiness detection.

The effect of MAR on the output is gradual and exhibits a lower slope compared with EAR. When the eyes are open (high EAR), increasing MAR leads to only a modest increase in the output value. This aligns with physiological patterns, as yawning alone is typically an early or mild indicator of fatigue and does not independently signify a critical drowsiness state. However, in the intermediate EAR range (approximately 0.25 – 0.35), the influence of MAR becomes more pronounced; higher MAR values result in a substantial increase in the drowsiness output. This behavior highlights the system’s ability to capture the progressive transition from alertness to drowsiness when both indicators jointly manifest moderate fatigue-related patterns.

The surface reveals a distinct nonlinear interaction between the two inputs. The combination of moderate EAR values with high MAR values produces significantly elevated output levels. This interaction reflects realistic behavioral dynamics, where partial eyelid drooping accompanied by repeated yawning is characteristic of intermediate or developing stages of drowsiness. The system’s representation of this synergy demonstrates that the fuzzy rule base effectively models the joint contribution of ocular and oral features to the overall assessment.

The presence of step-like transitions in the output surface indicates that the fuzzy system employs piecewise membership functions and discretized linguistic categories (e.g., Low, Medium, High). Such discontinuities are typical in Mamdani-type inference systems, where rule boundaries produce clearly defined transitions between different output regions.

This structured behavior confirms that the rule set and membership design partition the input space into meaningful regions, enabling the system to provide interpretable and logically consistent responses across varying levels of EAR and MAR.

The analysis of the sensitivity surface demonstrates that:

- EAR is the dominant indicator and strongly modulates the output, especially in regions associated with eye closure.
- MAR exerts a secondary but meaningful influence, particularly in intermediate drowsiness states.
- The fuzzy system captures nonlinear interactions between inputs, reflecting realistic behavioral patterns.
- The stepwise nature of the surface is consistent with the structure of linguistic rules in Mamdani inference.

Overall, the surface confirms that the fuzzy inference system accurately models the complex and progressive characteristics of human drowsiness based on facial behavior.

In the sensitivity plot, the color scheme reflects the degree of drowsiness, with green representing alertness (no drowsiness), yellow indicating moderate drowsiness, and red denoting severe drowsiness.

The driver’s drowsiness level was determined using Mamdani inference combined with the centroid method, with the output variable y and its associated membership degree calculated accordingly (equation (6)). Sample values from real-world data used for the calculation and validation of this output are provided in Tables 6 and 7 (equation (6)).

$$y^* = \frac{\sum (\mu(y) \cdot y)}{\sum \mu(y)} \tag{6}$$

The inference computations, derived from the sum of weights and the sum of membership functions presented in Tables 6 and 7, are as follows:

$$\begin{cases} \sum (\mu(y) \cdot y) = 0.32 + 0.50 + 0.42 = 1.24 \\ \sum \mu(y) = 0.8 + 1.0 + 0.7 = 2.5 \end{cases} \Rightarrow y^* = \frac{1.24}{2.5} = 0.5$$

$$\begin{cases} \sum (\mu(y) \cdot y) = 0.36 + 0.63 + 0.80 = 1.79 \\ \sum \mu(y) = 0.6 + 0.9 + 1.0 = 2.5 \end{cases} \Rightarrow y^* = \frac{1.79}{2.5} = 0.7$$

For all values of y within the range [0, 1], the levels of moderate and severe drowsiness are computed using the sum of weights and the sum of membership functions as follows:

$$\begin{cases} \sum (\mu(y) \cdot y) = 4.9495 \\ \sum \mu(y) = 9.8990 \end{cases} \Rightarrow y^* = \frac{4.9495}{9.8990} = 0.5$$

$$\begin{cases} \sum (\mu(y) \cdot y) = 6.9289 \\ \sum \mu(y) = 9.8990 \end{cases} \Rightarrow y^* = \frac{6.9289}{9.8990} = 0.7$$

Table 6. Sample values of Moderate Drowsiness.

| y value | Membership function $\mu(y)$ | Product $\mu(y) \cdot y$ |
|---------|------------------------------|--------------------------|
| 0.4 | 0.8 | 0.32 |
| 0.5 | 1.0 | 0.50 |
| 0.6 | 0.7 | 0.42 |

Table 7. Sample values of Severe Drowsiness.

| y value | Membership function $\mu(y)$ | Product $\mu(y) \cdot y$ |
|---------|------------------------------|--------------------------|
| 0.6 | 0.6 | 0.36 |
| 0.7 | 0.9 | 0.63 |
| 0.8 | 1.0 | 0.80 |

Using centroid-based inference, the overall levels of moderate and severe drowsiness are determined as follows:

$$\text{If : } \begin{cases} x = \text{Drowsiness} \\ y = \text{Level Drowsiness} \end{cases}$$

$$\Rightarrow y = \begin{cases} 0, & \text{if } 0.5 < x < 0.7 \text{ (Moderate Drowsiness)} \\ 1, & \text{if } x > 0.7 \text{ (Severe Drowsiness)}. \end{cases}$$

In the output of the Mamdani fuzzy inference system, a value of 0.5 denotes moderate drowsiness, whereas a value of 0.7 corresponds to severe drowsiness. Each individual's drowsiness level is updated and logged in an Excel spreadsheet. For storage, Mamdani output values between 0.5 and below 0.7 are recorded as 0 (moderate drowsiness), while values exceeding 0.7 are recorded as 1 (severe drowsiness). These entries are refreshed with each new test (Fig. 17). The fuzzy membership functions, combined rules, and Mamdani inference outputs are presented in Fig. 18. During drowsiness detection, the values in the table are updated in real time, and the system continuously refreshes the data instantaneously.

| A |
|------------|
| Drowsiness |
| 0 |

| A |
|------------|
| Drowsiness |
| 1 |

Figure 17. Saving Drowsiness results.

3. Results

All trained neural networks, their derived models, and the full image processing and fuzzy logic modules were implemented using Python in the PyCharm environment. Abbreviations are used in this section to streamline the expressions within the summary tables (Table 8). The participants took part in live video testing for an average duration of 5 minutes (ranging from 4 to 6 minutes). Yawning and eye drowsiness were examined. A total of 3,397,500 frames were collected for drowsiness detection. The live videos were fed into the system at a rate of 25 frames per second, and the system used a ResNet50-based deep neural network model to detect drowsiness. Furthermore, a combination of this model with fuzzy inference was employed to determine the level of drowsiness.

Table 9 summarizes the specifications of all neural networks trained for drowsiness detection with two labels: Normal and Drowsiness. Among them, the ResNet50 network achieved the highest training accuracy, the second-highest validation accuracy, the lowest training error rate, and the third-lowest validation error count. It also outperformed all other networks across

test metrics, including training and validation F1-scores, precision, and recall, as well as real-time inference performance. Consequently, ResNet50 was selected as the optimal neural network for distinguishing between Normal and Drowsiness labels.

The ResNet50-derived model, employed for field-testing drowsiness detection, demonstrated real-time processing capability for video frames on an RTX 3060 laptop GPU with 6GB RAM. A dedicated comparison of all trained models confirmed the superior performance of the ResNet50-based model. The inference models from each network were combined with EAR and MAR image processing techniques and fuzzy logic to both detect drowsiness and quantify its severity. All tests were conducted on an RTX 3060 laptop GPU with 6GB RAM to evaluate per-frame processing times (Table 10).

An important observation in Table 9 and 10 is that the ViT-Tiny and MobileNetV3 networks, which showed the weakest training performance, achieved the fastest real-time image processing among all models. This outcome is attributed to their poor training results, where lower accuracy translated into faster execution. However, because of their inadequate accuracy, these networks were excluded from the comparative analysis reported in Table 11.

At the conclusion of this section, the ResNet50 neural network is identified as the best-performing model. To further validate its effectiveness, it is compared with related studies conducted by other researchers to assess whether it also surpasses similar approaches (Table 11).

The comparison between the ResNet50 neural network implemented in this study and other related works demonstrated the clear superiority of the model developed in this research. Furthermore, the research gap and the necessity of implementing the proposed method were highlighted in a comprehensive comparison (Table 12).

The field evaluation of the integrated system for drowsiness detection and severity estimation was carried out with 453 volunteers representing diverse Middle Eastern ethnic groups, including Azerbaijani, Gilaki, Mazandarani, Lur, Kurdish, Turkmen, Baluchi, Tajik, Hazara, and Arab. To address the challenge of fluctuating lighting conditions, an infrared camera was employed, allowing the system to automatically switch to infrared illumination when required. Among the 453 trials, 31 errors were recorded, yielding an overall system accuracy of 93.16% (Fig. 19, Table 13). Fuzzy and intelligent approaches for drowsiness detection and related systems were examined in a comprehensive review (Table 14).

Although the accuracy of the combined system is slightly lower than that reported in other similar works (Table 9), those studies did not include large-scale implementation or field testing. In contrast, this study validated its results through extensive evaluation with 453 participants, ensuring the reliability of the findings.

The causes of system errors were documented and analyzed in four distinct scenarios:

- Scenario 1: When a person is shouting, the system may misinterpret it as yawning. In other cases,

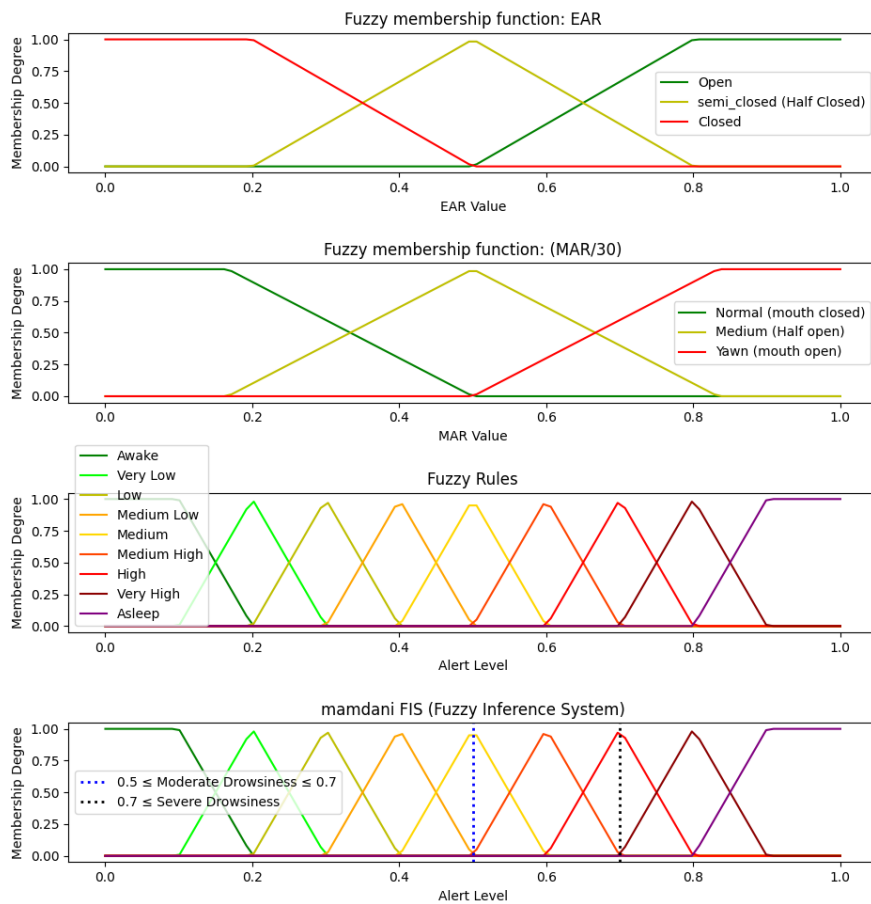


Figure 18. Membership functions and fuzzy system inference engine in real-time detection of Drowsiness level.

yawning is detected correctly (Fig. 20 (a)).

- Scenario 2: Accurate drowsiness detection requires both eyes of the driver to be visible. If not, the system classifies the driver as normal (non-drowsy). In some cases, even face detection and recognition fail (Fig. 20 (b)).
- Scenario 3: Wearing a face mask prevents the system from recognizing yawning. Since the image is captured from a frontal view, the system attempts

to estimate facial landmarks but cannot determine mouth status. As a result, it defaults to classifying the mouth as closed (normal) (Fig. 20 (c)).

- Scenario 4: When the driver wears sunglasses, detection accuracy depends on the infrared camera. If IR light passes through and the eyes are visible, detection is correct; otherwise, the system identifies the driver as normal (non-drowsy) (Fig. 20 (d)).

To further examine the contribution of each component within the proposed architecture, an ablation-style

Table 8. Abbreviations.

| Abbreviation: expression | Abbreviation: expression | Abbreviation: expression |
|-----------------------------|-----------------------------|-----------------------------------|
| P: Parameters | VP: Validation precision | CHP: CNN + HOG + PCA |
| TA: Training accuracy (%) | TR: Training recall | DS: DCCNN + SVM |
| VA: Validation accuracy (%) | VR: Validation recall | SN: Shallow CNN |
| TL: Training loss | RI: Real-Time inference (s) | CL: CNN-LSTM |
| VL: Validation loss | R50: ResNet50 | MKBY: MC-KFC + blinking + yawning |
| TF: Training F1-score | M: MobileNetV3 | 3DF: 3D 478 FFLs (Face Mesh) |
| VF: Validation F1-score | VT: ViT-Tiny | MN: MobileNet |
| TP: Training precision | NV: Novel VGLG | R50FF: ResNet50 + Fuzzy FIS |

Table 9. Neural networks results.

| P | R50 | M | VT |
|----|-------|-------|-------|
| TA | 99.74 | 99.08 | 98.62 |
| VA | 99.62 | 96.84 | 98.46 |
| TL | 0.006 | 0.022 | 0.034 |
| VL | 0.022 | 0.106 | 0.077 |
| TF | 0.99 | 0.99 | 0.98 |
| VF | 0.99 | 0.96 | 0.98 |
| TP | 0.99 | 0.99 | 0.98 |
| VP | 0.99 | 0.97 | 0.98 |
| TR | 0.99 | 0.99 | 0.98 |
| VR | 0.99 | 0.96 | 0.98 |
| RI | 0.023 | 0.021 | 0.021 |

Table 10. Real-time process on RTX3060 laptop GPU.

| Inference method | Real-Time (s) |
|---------------------|---------------|
| ResNet50 + Fuzzy | FIS 0.023 |
| ViT-Tiny + Fuzzy | FIS 0.021 |
| MobileNetV3 + Fuzzy | FIS 0.021 |

analysis was incorporated into the manuscript. The system was evaluated in three configurations: (1) using the deep neural network alone, (2) using only the EAR/MAR-based fuzzy inference system, and (3) using the full hybrid model. The results indicate that while the ResNet50 model provides highly accurate binary detection, the hybrid model enhances robustness in ambiguous visual conditions and enables reliable estimation of drowsiness severity. Additionally, the comparative analysis section was expanded with transformer-based and state-of-the-art deep learning approaches to provide a more comprehensive performance benchmark. Moreover, a detailed discussion of real-time implementation

constraints was added, covering limitations related to GPU dependency, eye occlusion, face masks, IR illumination, head movements, and confusion between yawning and speech. These additions strengthen the scientific rigor of the manuscript and directly address the ablation analysis, benchmarking, and real-time implementation constraints.

This study centers on the implementation of the ResNet50 neural network with a highly practical architecture for training a drowsiness dataset. The network design incorporates convolutional layers with ReLU activation and MaxPooling, followed by a fully connected layer using a sigmoid activation function with two out-

Table 11. Comparison of Drowsiness detection results.

| Ref. | Method | TA | Recall | Precision | TF |
|-----------|--------|-------|--------|-----------|-------|
| [1] | NV | 99 | 0.99 | 0.99 | 0.99 |
| [2] | ViT | 99.4 | - | - | - |
| [3] | Swin | 99.82 | - | - | - |
| [4] | CHP | 99.6 | 0.968 | 0.597 | 0.738 |
| [5] | DS | 94.8 | - | - | - |
| [6] | GAN | 98.01 | - | - | - |
| [7] | SN | 99.23 | 1 | 0.99 | 0.99 |
| [8] | CL | 96 | 0.95 | 0.95 | 0.95 |
| [9] | MKBY | 93.6 | - | - | - |
| [10] | 3DF | 84 | - | - | - |
| [11] | CNN | 98.2 | 0.81 | 0.92 | 0.86 |
| [12] | MN | 99.94 | 0.99 | 0.99 | 0.99 |
| This work | R50 | 99.74 | 0.99 | 0.99 | 0.99 |

Table 12. Comparison of recent studies on driver Drowsiness detection with the proposed method.

| Ref. | Year | Method | Dataset | Features/Modalities | Evaluation metrics | Main findings |
|-----------|------|---|--|--|---------------------------------------|---|
| [1] | 2024 | Transfer Learning (TL) | Eye movement dataset (proprietary) | Eye Movement behavior | Accuracy, F1 | Proposed TL model outperforms baselines in eye-based drowsiness detection |
| [2] | 2025 | Vision Transformer (ViT-DDD) | NTHU-DDD, UTA-RLDD | Full-Face image (non-intrusive vision) | Accuracy | ViT-based system achieves 98.89%-99.4%, robust to glasses, sunglasses, lighting changes; real-time raspberry pi deployment |
| [3] | 2025 | Swin Transformer + Diffusion Model | Eye-Blink, CEW | Eye-region images + diffusion denoising | Accuracy, Precision, Recall, F1, | Achieves 99.82%-99.94% accuracy; highly robust to noise & adversarial attacks (FGSM/PGD); diffusion improves visual quality |
| [4] | 2024 | Hybrid Deep Learning | Custom dataset | Facial + behavioral features | Accuracy | Hybrid DL achieves higher accuracy than single CNNs |
| [5] | 2019 | Real-time CNN | NTHU-DDD | Facial landmarks + PERCLOS | Accuracy, ROC | Considers individual differences; good generalization |
| [6] | 2020 | GANs for bias reduction | N/A | Facial images | Accuracy | GAN reduces bias in drowsiness detection |
| [7] | 2024 | Lightweight CNN (Drowsy-DetectNet) | Limited-size dataset | Facial features | Accuracy, Precision | Performs well with small training data |
| [8] | 2024 | Data Fusion (multimodal) | Multimodal dataset | EEG + Eye + Video | Accuracy, Recall | Fusion improves recognition compared to single modality |
| [9] | 2019 | Real-time CNN | NTHU-DDD | Facial features | Accuracy | Achieves reliable real-time detection |
| [10] | 2025 | Thermal + CNN | Thermal face dataset | FaceMesh landmarks | Accuracy | Reduces face orientation effects |
| [11] | 2023 | Edge-based ML | Mobile edge dataset | Video + sensors | Accuracy, Latency | Real-time edge deployment feasible |
| [12] | 2024 | TL + CNN | Transfer learning dataset | CNN features | Accuracy | Improves recognition speed |
| [13] | 2024 | Dual-Modal Detection | Multimodal dataset | Video + Physiological | Accuracy, Precision | Improves driver safety with two modalities |
| [14] | 2019 | Survey | N/A | Survey | N/A | Comprehensive survey of techniques |
| [15] | 2022 | CNN + Multi-aspect Image Processing (EAR, MAR, FAR, gradient-based orientation) | NTHU-DDD, YawDD, EMOCDS, UTA-RLDD | Eye, Mouth, Face landmarks + Hand gestures + Orientation | Accuracy, TP/TN/FPP/FN analysis | Proposed integrated system detects drowsiness from multiple aspects (eye closure, yawning, hand on face, sunglasses, face orientation). Outperforms state-of-the-art methods under varying illumination and scenarios |
| This work | 2025 | Hybrid Real-time CNN + Fuzzy | Driver Drowsiness Detection (Roboflow, Ito-mic01); 453 real test samples | Live camera: CNN features + Facial landmarks (EAR, MAR) | Accuracy, Precision, Recall, F1-Score | The system demonstrated very high accuracy performance under varying lighting conditions, even with participants from different ethnic backgrounds during the field test. |



Figure 19. Examples of Field Tests.

put neurons to maximize classification accuracy for the dataset. The ResNet50 network achieved a training accuracy of 99.74% with minimal errors in both training and validation phases. By integrating the trained model with image processing methods based on EAR and MAR metrics, along with fuzzy logic, a unified system was developed capable of processing video frames in real time. To further assess its ability to determine drowsiness severity, the combined system was tested in field experiments with 453 participants. The results indicated an accuracy of 93.16%, with 31 error cases.

The primary sources of error were identified as: incomplete visibility of both eyes in the image, face masks obscuring the mouth, sunglasses resistant to infrared transmission, and shouting, which interfered with yawning detection.

This reduction mainly arises from uncertainty propagation during fuzzification, threshold-based membership mapping, and the aggregation of multiple inputs

to estimate drowsiness intensity rather than performing binary classification alone. Nevertheless, the hybrid CNN–fuzzy framework enables real-time detection along with interpretable estimation of drowsiness levels, enhancing system robustness in practical scenarios. While the CNN-only model achieves higher classification accuracy under controlled conditions, a slight performance reduction is observed after integration with the fuzzy inference system and real-world deployment.

Despite the continuous release of more powerful processors, this study adopted a cost-effective approach by utilizing an RTX 3060 laptop GPU with 6GB RAM for all training and testing. The proposed system's capabilities can be replicated on similar GPUs, offering real-time, high-accuracy image processing for both detecting and evaluating driver drowsiness. Given its proven accuracy and real-world reliability, the system has strong potential for future integration into in-vehicle image processing units within advanced driver-assistance systems (ADAS).

Table 13. Output results in Drowsiness level detection.

| Ref. | Method | Result Accuracy (%) |
|----------------|--------|---------------------|
| [25] | NV | 95.5 |
| [26] | CHP | 97.5 |
| [27] | DS | 97.5 |
| [28] | GAN | 94.5 |
| Proposed paper | R50FF | 93.16 |

Table 14. Fuzzy and intelligent approaches for drowsiness & related systems.

| Ref. | Year | Application | Method | Contribution |
|-----------|------|--------------------|-----------------------------|---|
| [25] | 2019 | Driver drowsiness | Fuzzy Inference System | Introduced fuzzy rules for real-time drowsiness |
| [26] | 2020 | Driver drowsiness | Portable Fuzzy System | Portable system for fuzzy-based drowsiness |
| [27] | 2025 | Driver drowsiness | Multi-feature + Fuzzy Logic | Intelligent fuzzy system for feature selection |
| [28] | 2022 | Driver drowsiness | Fuzzy + Image Processing | Enhanced detection via fuzzy optimization |
| [29] | 2019 | UAV (Quadrotor) | Sliding Mode + Fuzzy | Improved control via fuzzy-based augmentation |
| [30] | 2012 | EMG signals | Adaptive Laguerre + Fuzzy | Eliminates power line noise with fuzzy step-size |
| [31] | 2020 | Casting machines | PI + Fuzzy Controller | Hydraulic servo-valve control using fuzzy PI |
| [32] | 2017 | Power distribution | Fuzzy DSTATCOM | Power quality improvement |
| [33] | 2025 | Solar panels | Recursive + Fuzzy | Fault diagnosis in solar systems |
| [34] | 2014 | Clustering | Hybrid GA-PSO + Fuzzy | Automatic clustering optimization |
| [35] | 2010 | Video compression | Fuzzy Motion Estimation | Improved motion estimation |
| [36] | 2010 | Image denoising | Genetic + Fuzzy filter | Impulse noise removal |
| [37] | 2013 | Image processing | Fuzzy Edge Detection | Edge detection in noisy images |
| This work | 2025 | Driver drowsiness | Hybrid Real-time CNN +Fuzzy | Combines real-time CNN with fuzzy rules; tested on 453 real-world driver samples for practical accuracy |

**Figure 20.** Scenario 1, 2, 3, 4.

4. Conclusion

The aim of this research was to address aspects overlooked in similar studies, such as conducting field tests with volunteers from diverse ethnic backgrounds, testing under varying lighting conditions, using uniform and cost-effective hardware, and ensuring the practical applicability of the study. All these objectives were addressed through the proposed hybrid approach combining a convolutional neural network and fuzzy inference, offering the added advantage of real-time processing. To maintain real-time processing relationships in the paper when implementing on lower-performance hardware, it is suggested to reduce the number of frames received

from the camera. This number should not be set below 10 frames per second. The reason is that if the number of received frames falls below a certain threshold, the system's sensitivity in real-time detection under actual conditions will decrease. While the real-time experiments were conducted on an RTX 3060 GPU, the proposed framework can be adapted for deployment on embedded platforms (e.g., Raspberry Pi) by applying model compression, resolution reduction, or lightweight network variants, albeit with a trade-off in inference speed and accuracy.

Acknowledgement

We extend our appreciation to the students (from various ethnic groups) of the Faculty of Engineering at the Islamic Azad University, Y.I.C., who voluntarily participated in the field testing of the real-time drowsiness detection image processing system. All participants were fully aware that their facial images would be published in the research article and provided their consent.

Authors contributions

All authors contributed equally to the conception, design, execution, and writing of this work. All authors read and approved the final manuscript.

Availability of data and materials

The authors declare that the data supporting the findings of this study are available within the paper.

Conflict of interests

The authors assert that they do not have any identifiable conflicting financial interests or personal relationships that might be perceived to influence the work presented in this paper.

References

- Madni HA, Raza A, Sehar R, Thalji N, and Abualigah L. "Novel Transfer Learning Approach for Driver Drowsiness Detection Using Eye Movement Behavior." *IEEE* 2024; 12:64765–78. DOI: [10.1109/ACCESS.2024.3522111](https://doi.org/10.1109/ACCESS.2024.3522111)
- Jarndal A, Tawfik H, Siam AI, Alsyof I, and Cheaitou A. "A Real-Time Vision Transformers-Based System for Enhanced Driver Drowsiness Detection and Vehicle Safety." *IEEE* 2025; 13:1790–803. DOI: [10.1109/ACCESS.2024.3522111](https://doi.org/10.1109/ACCESS.2024.3522111)
- El-Nabi SA et al. "Driver Drowsiness Detection Using Swin Transformer and Diffusion Models for Robust Image Denoising." *IEEE* 2025; 13:71880–907. DOI: [10.1109/ACCESS.2025.3561717](https://doi.org/10.1109/ACCESS.2025.3561717)
- Ramzan M, Abid A, Fayyaz M, Alahmadi TJ, Nobanee H, and Rehman A. "A Novel Hybrid Approach for Driver Drowsiness Detection Using a Custom Deep Learning Model." *IEEE* 2024; 12:126866–84. DOI: [10.1109/ACCESS.2024.3438617](https://doi.org/10.1109/ACCESS.2024.3438617)
- You F, Li X, Wang YGH, and Li H. "A Real-time Driving Drowsiness Detection Algorithm with Individual Differences Consideration." *IEEE* 2019; 7:179396–408. DOI: [10.1109/ACCESS.2019.2958667](https://doi.org/10.1109/ACCESS.2019.2958667)
- Ngxande M, Tapamo JR, and Burke M. "Bias Remediation in Driver Drowsiness Detection Systems Using Generative Adversarial Networks." *IEEE* 2020; 8:55592–601. DOI: [10.1109/ACCESS.2020.2981912](https://doi.org/10.1109/ACCESS.2020.2981912)
- Venkateswarlu M and Ch VRR. "DrowsyDetectNet: Driver Drowsiness Detection Using Lightweight CNN With Limited Training Data." *IEEE* 2024; 12:110476–91. DOI: [10.1109/ACCESS.2024.3440585](https://doi.org/10.1109/ACCESS.2024.3440585)
- Priyanka S, Shanthi S, Kumar AS, and Praveen V. "Data fusion for driver drowsiness recognition: A multimodal perspective." *Egyptian Informatics Journal* 2024; 27. DOI: [10.1016/j.eij.2024.100529](https://doi.org/10.1016/j.eij.2024.100529)
- Deng W and Wu R. "Real-Time Driver-Drowsiness Detection System Using Facial Features." *IEEE* 2019; 7:118727–38. DOI: [10.1109/ACCESS.2019.2936663](https://doi.org/10.1109/ACCESS.2019.2936663)
- Nomura A, Yoshida A, Nagumo K, and Nozawa A. "Reducing the effect of face orientation using FaceMesh landmarks in drowsiness estimation based on facial thermal images." *Nature* 2025; 30:317–24. DOI: [10.1007/s10015-024-01001-1](https://doi.org/10.1007/s10015-024-01001-1)
- Lamaazi H, Alqassab A, Fadul RA, and Mizouni R. "Smart Edge-Based Driver Drowsiness Detection in Mobile Crowdsourcing." *IEEE* 2023; 11:21863–72. DOI: [10.1109/ACCESS.2023.3250834](https://doi.org/10.1109/ACCESS.2023.3250834)
- Salem D and Waleed M. "Drowsiness detection in real-time via convolutional neural networks and transfer learning." *Journal of Engineering and Applied Science* 2024; 71. DOI: [10.1186/s44147-024-00457-z](https://doi.org/10.1186/s44147-024-00457-z)
- Chew YX, Razak SFA, Yogarayan S, and Ismail SNMS. "Dual-Modal Drowsiness Detection to Enhance Driver Safety." *Computers, Materials & Continua* 2024; 81:4397–417. DOI: [10.32604/cmc.2024.056367](https://doi.org/10.32604/cmc.2024.056367)
- Ramzan M, Khan HU, Awan SM, Ismail A, Ilyas M, and Mahmood A. "A Survey on State-of-the-Art Drowsiness Detection Techniques." *IEEE* 2019; 7:61904–19. DOI: [10.1109/ACCESS.2019.2914373](https://doi.org/10.1109/ACCESS.2019.2914373)
- Maheswari VU, Aluvalu R, Kantipudi MP, Chenam KK, Kotecha K, and Saini JR. "Driver Drowsiness Prediction Based on Multiple Aspects Using Image Processing Techniques." *IEEE* 2022; 10:54980–90. DOI: [10.1109/ACCESS.2022.3176451](https://doi.org/10.1109/ACCESS.2022.3176451)
- Yadav A, Hussain R, Shukla M, J. B RK, Mary SP, Hsu C, Mishra MK, Saleem K, and El-Meligy M. "Enhancing convolutional neural networks in electroencephalogram driver drowsiness detection using human inspired optimizers." *Scientific Reports* 2025; 15. DOI: [10.1109/ACCESS.2022.3187995](https://doi.org/10.1109/ACCESS.2022.3187995)
- Murata A, Doi T, and Karwowski W. "Sensitivity of PERCLOS70 to Drowsiness Level: Effectiveness of PERCLOS70 to Prevent Crashes Caused by Drowsiness." *IEEE* 2022; 10:70806–14. DOI: [10.1109/ACCESS.2022.3187995](https://doi.org/10.1109/ACCESS.2022.3187995)

18. Cai J, Liao X, Bai J, Luo Z, Li L, and Bai J. **“Face Fatigue Feature Detection Based on Improved D-S Model in Complex Scenes.”** *IEEE* 2023; 11:101790–8. DOI: [10.1109/ACCESS.2023.3314665](https://doi.org/10.1109/ACCESS.2023.3314665)
19. Mohammed AZ, Mohammed EA, and Aaref AM. **“Real-Time Driver Awareness Detection System.”** *IOP Conference Series: Materials Science and Engineering* 2020; 745. DOI: [10.1088/1757-899X/745/1/012053](https://doi.org/10.1088/1757-899X/745/1/012053)
20. Nagdeote S, Pendhari H, John M, and Agrawal S. **“An Approach to Detect Driver Drowsiness in Real Time using Facial Landmarks.”** *SAMRID-DHI: A Journal of Physical Sciences, Engineering and Technology* 2023; 15. DOI: [10.18090/samriddhi.v15i01.21](https://doi.org/10.18090/samriddhi.v15i01.21)
21. Titare S, Chinchghare S, and Hande KN. **“Driver Drowsiness Detection and Alert System.”** *International Journal of Scientific Research in Computer Science, Engineering and Information Technology (ISJRCSEIT)* 2021; 7:583–8. DOI: [10.32628/CSEIT2173171](https://doi.org/10.32628/CSEIT2173171)
22. Alshamrani R, Alshehri F, and Kurdi H. **“A Pre-processing Technique for Fast Convex Hull Computation.”** *Procedia Computer Science* 2020; 170:317–24. DOI: [10.1016/j.procs.2020.03.046](https://doi.org/10.1016/j.procs.2020.03.046)
23. Adarsh G, Singh V, Singh S, and Hazela B. **“Drowsiness Detection System in Real Time Based on Behavioral Characteristics of Driver using Machine Learning Approach.”** *Journal of Informatics Electrical and Electronics Engineering (JIEEE)* 2023; 04:1–10. DOI: [10.54060/jieee.v4i1.84](https://doi.org/10.54060/jieee.v4i1.84)
24. Asdyo B, Kanigoro B, and Rojali. **“Drowsy Detection System by Facial Landmark and Light Gradient Boosting Machine Method.”** *Procedia Computer Science* 2023; 277:500–7. DOI: [10.1016/j.procs.2023.10.551](https://doi.org/10.1016/j.procs.2023.10.551)
25. Wang L, Wang H, and Liu J. **“Discrimination of Driver Fatigue Based on Distortion Energy Density Theory and Multiple Physiological Signals.”** *IEEE* 2021; 9:151824–33. DOI: [10.1109/ACCESS.2021.3125052](https://doi.org/10.1109/ACCESS.2021.3125052)
26. Celecia A, Figueiredo K, Vellasco M, and Gonzalez R. **“A Portable Fuzzy Driver Drowsiness Estimation System.”** *Sensors* 2020; 20. DOI: [10.3390/s20154093](https://doi.org/10.3390/s20154093)
27. Arava M and Sundaram DM. **“Multi-Figure Selection and Fuzzy Logic-Based Intelligent Driver Drowsiness Detection.”** *Institution of Engineering and Technology (IET)* 2025; 19. DOI: [10.1049/ipr2.70052](https://doi.org/10.1049/ipr2.70052)
28. Alkishri W, Abualkishik A, and Al-Bahri M. **“Enhanced Image Processing and Fuzzy Logic Approach Optimizing Driver Drowsiness Detection.”** *Applied Computational Intelligence and Soft Computing* 2022; 2022. DOI: [10.1155/2022/9551203](https://doi.org/10.1155/2022/9551203)
29. Sorourkhah A. **“Coping Uncertainty in the Supplier Selection Problem Using a Scenario-Based Approach and Distance Measure on Type-2 Intuitionistic Fuzzy Sets.”** *Fuzzy Optimization and Modelling* 2022; 3:1–8. DOI: [10.30495/fomj.2022.1953705.1066](https://doi.org/10.30495/fomj.2022.1953705.1066)
30. Khaniki MAL, Hadi MB, and Manthouri M. **“Tuning of Novel Fractional Order Fuzzy PID Controller for Automatic Voltage Regulator using Grasshopper Optimization Algorithm.”** *Majlesi Journal of Electrical Engineering* 2012; 15. DOI: [10.52547/mjee.15.2.39](https://doi.org/10.52547/mjee.15.2.39)
31. Jalali M, Kardehi R, and Pariz N. **“Maximum Energy Absorbed from the Persian Gulf Waves Considering Uncertainty in Power Take off Parameters.”** *Majlesi Journal of Electrical Engineering* 2022; 16. DOI: [10.30486/mjee.2022.696491](https://doi.org/10.30486/mjee.2022.696491)
32. Abadi DNM, Moarefianpopur A, and Dehkordi NM. **“Finite-Time Bounded Model-Based Event-Triggered Control for Distributed Fuzzy T-S Systems.”** *Majlesi Journal of Electrical Engineering* 2024; 18. DOI: [10.30486/mjee.2023.1994207.1226](https://doi.org/10.30486/mjee.2023.1994207.1226)
33. Boulanouar S and Boualem F. **“Solar panel fault diagnosis based on the intelligent recursive method.”** *Majlesi Journal of Electrical Engineering* 2025; 19. DOI: [10.57647/j.mjee.2025.1902.28](https://doi.org/10.57647/j.mjee.2025.1902.28)
34. Janah NZ and Baharudin B. **“Genetic Fuzzy Filter Based on MAD and ROAD to Remove Mixed Impulse Noise.”** *Majlesi Journal of Electrical Engineering* 2010; 4. DOI: [10.1234mjee.v4i2.283](https://doi.org/10.1234mjee.v4i2.283)
35. Soroushmehr SM. **“A New Fuzzy Based Motion Estimation Algorithm in Video Compression.”** *Majlesi Journal of Electrical Engineering* 2010; 4. DOI: [10.1234mjee.v4i2.197](https://doi.org/10.1234mjee.v4i2.197)
36. Ghaleh OD, Maihami V, and Khamforoosh K. **“A Hybrid Method for Medical Image Denoising and Segmentation Using Optimized Fuzzy Clustering and Autoencoder.”** *Fuzzy Optimization and Modeling Journal (FOMJ)* 2025; 6. DOI: [10.57647/j.fomj.2025.0602.10](https://doi.org/10.57647/j.fomj.2025.0602.10)
37. Sakhaei SF, Afshari AJ, Bosaghzade A, and Jahromi MHM. **“Intelligent Image-Based Recognition of Rice Cultivars Using PSO-Optimized ANFIF.”** *Fuzzy Optimization and Modeling Journal (FOMJ)* 2025; 6. DOI: [10.57647/j.fomj.2025.0603.17](https://doi.org/10.57647/j.fomj.2025.0603.17)